A novel miniature dynamic microfluidic cell culture platform using electro-osmosis diode pumping

Jen-Yung Chang (仁勇 張),[1,a)] Shuo Wang (碩 王),[1,a)] Jeffrey S. Allen,[1]
Seong Hyuk Lee,[2] Suk Tai Chang,[3] Young-Ki Choi,[2] Craig Friedrich,[1]
and Chang Kyoung Choi[1,b)]

[1]*Department of Mechanical Engineering-Engineering Mechanics, Michigan Technological University, Houghton Michigan 49931, USA*
[2]*School of Mechanical Engineering, Chung-Ang University, 221 Heukseok-Dong, Dongjak-Gu, Seoul 156-756, South Korea*
[3]*School of Chemical Engineering and Materials Science, Chung-Ang University, 221 Heukseok-Dong, Dongjak-Gu, Seoul 156-756, South Korea*

An electro-osmosis (EOS) diode pumping platform capable of culturing cells in fluidic cellular micro-environments particularly at low volume flow rates has been developed. Diode pumps have been shown to be a viable alternative to mechanically driven pumps. Typically electrokinetic micro-pumps were limited to low-concentration solutions (≤ 10 mM). In our approach, surface mount diodes were embedded along the sidewalls of a microchannel to rectify externally applied alternating current into pulsed direct current power across the diodes in order to generate EOS flows. This approach has for the first time generated flows at ultra-low flow rates (from 2.0 nl/s to 12.3 nl/s) in aqueous solutions with concentrations greater than 100 mM. The range of flow was generated by changing the electric field strength applied to the diodes from 0.5 Vpp/cm to 10 Vpp/cm. Embedding an additional diode on the upper surface of the enclosed microchannel increased flow rates further. We characterized the diode pump-driven fluidics in terms of intensities and frequencies of electric inputs, pH values of solutions, and solution types. As part of this study, we found that the growth of A549 human lung cancer cells was positively affected in the microfluidic diode pumping system. Though the chemical reaction compromised the fluidic control overtime, the system could be maintained fully functional over a long time if the solution was changed every hour. In conclusion, the advantage of miniature size and ability to accurately control fluids at ultra-low volume flow rates can make this diode pumping system attractive to lab-on-a-chip applications and biomedical engineering *in vitro* studies. © *2014 AIP Publishing LLC*. [http://dx.doi.org/10.1063/1.4892894]

I. INTRODUCTION

In the human body, bio-physiological mechanical stimulants, such as shear forces from blood flow, influence the physiology of cells. As such, *in vivo* testing is often preferred over *in vitro* experiments (i.e., a controlled environment within a Petri-dish or test tube). However, *in vivo* testing is more expensive, inherently more variable, and requires federal approval to mitigate harm to test subjects. Therefore, *in vitro* models have various advantages in biomedical research areas. It is easier and/or safer for *in vitro* models to control parameters and observe results than that *in vivo*, especially when employing potentially hazardous or untried protocols. However, one inherent deficiency for static *in vitro* models using culture dish/plate is the potential to oversimplify the complex and dynamic fluidic nature of *in vivo* environments.[1,2] The

---

a)J.-Y. Chang and S. Wang contributed equally to this work.
b)Author to whom correspondence should be addressed. Electronic mail: cchoi@mtu.edu

lack of fluid flow conditions in the *in vitro* culturing methods may compromise the results. Specifically, non-uniform distribution of molecules in a static *in vitro* model may result in local deviation of results and potentially increase unnecessary cell movement to the most abundant source of nutrients.[3] In addition, fluid flow shears can significantly regulate the metabolism of certain types of cells, such as endothelial and smooth muscle cells in blood vessels,[4,5] fibroblasts in muscles,[6,7] bone cells,[8,9] and chondrocytes in articular cartilages.[10,11] Subsequently, fluidic flow conditions are favorable for these types of cells to live *in vivo*. There are an increasing number of studies that employ dynamic flow environments for *in vitro* models for bio-related research, such as DNA sequencing, and cell manipulation and sorting.[12–14]

Fluid driving/pumping systems are the essential part for bio-microfluidic devices to control precise and stable fluid flows. A number of technologies were developed based on different mechanisms—piezoelectric,[15] pneumatic,[16] peristaltic,[17] centrifugal,[18] electrostatic,[19] ultrasonic,[20] and magneto-hydrodynamic effects.[21] Mechanically driven pumps require relatively large hardware devices and equipment.[22] These pumps are limited for lab-on-a-chip applications. In addition, the scale limitation also makes it challenging to control flows at ultra-low volume flow rates.

Diode pumping technology, based on electro-osmosis (EOS), has shown promise to overcome the pumping issues described.[23] Electro-osmosis flows (EOFs) can be generated using either an alternating current (AC) or direct current (DC). DC electro-osmosis (DCEO) can be applied to create single-direction flows through the electric potential. In microfluidic channels, DCEO systems are well-suited to control pulse, continuous or other types of flows. However, DCEO may change the chemical composition of electrolyte solutions via electrolysis and make it difficult to control the flow, which indicates that the DCEO system is not suitable for biomedical microfluidics due to the presence of nutrition and metabolic products.[24] In contrast, an AC electro-osmosis (ACEO) micro-pump that uses asymmetrical electrode configurations has been proven to minimize electrolysis.[25] However, the issues of complex fabrication of thin film electrodes or the imprecise control of steady flows has not been addressed in ACEO pumps.[26–28] Recently, a surface mount diode (SMD) in microfluidic pumping and mixing systems was proposed to rectify AC to DC to easily control the flow types without complicated fabrication.[29] The mechanism of SMD pumping is that the SMD rectifies AC to DC to make the AC signal dissymmetric, which generates the DCEO by DC-bias on the SMD surface. The localized DC EOF on the diode surface generates the pressure gradient across the diode. This pressure gradient eventually pumps the fluids through the other sections of the microchannel. However, it was unknown whether this pumping approach could be employed for cell culture applications, where saline concentrations can be relatively high ($>10\,\mathrm{mM}$) in the culture medium.[30] Therefore, this study aimed to design a diode pumping system to generate steady flows with ultra-low flow rates in high-concentration ($100\,\mathrm{mM}$) saline solutions of potassium chloride (KCl) or sodium chloride (NaCl). Both experimental study and computational fluid dynamics (CFD) were employed to characterize fluidics generated by diode pumping. Another objective was to identify the biocompatibility of our diode pumping system compared to a traditional syringe pump.

II. METHODS AND EXPERIMENTS

A. Design and fabrication of a diode pumping culture platform

The schematic of the diode pumping culture platform is in Figure 1(a). Polydimethylsiloxane (PDMS, Sylgard 184, Dow Corning, MI) microfluidic channels with $800\,\mu\mathrm{m}$ (W) $\times$ $650\,\mu\mathrm{m}$ (H) cross-section were first fabricated on a $75\,\mathrm{mm} \times 25\,\mathrm{mm}$ slide glass substrate using photolithography.[16,31] The overall dimensions of the microchannel are $70\,\mathrm{mm}$ (L) $\times$ $20\,\mathrm{mm}$ (W). The radius of the turning section is $10\,\mathrm{mm}$. The distance between the electrodes is $10\,\mathrm{mm}$ (see Fig. 1(a)). Inlet and outlet are on both sides of the microchannel for inputting/outputting fluids, changing medium, and inoculating cells. SMDs (1N4448HWTDICT-ND, SOD-523, Digi-Key, MN) were embedded along the channel between two 21-gauge needles that function as electrodes (note that the distance between the electrodes was $10\,\mathrm{mm}$ for all
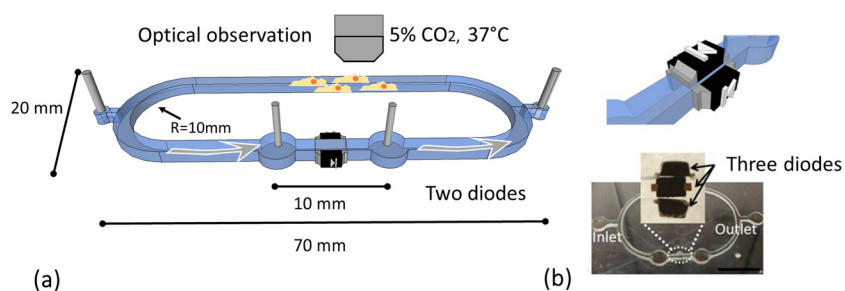
FIG. 1. Schematic of an AC diode pumping culture platform and corresponding photographs. Two-diode (a) and three-diode pumps (b) were shown. Scale bar $= 10$ mm.

experiments expect the cell culturing experiment with 8 mm separation). Two configurations of the diode pumping system were fabricated (Figures 1(a) and 1(b)). For the two-diode configuration, two SMDs were embedded along the two PDMS sidewalls; whereas for the three-diode version, one additional diode was embedded in parallel on the upper surface of the enclosed microchannel to increase the flow rate. Note that the electric signals were directly applied on the diodes via the electrolyte in the microchannel. Therefore, no additional electrical connections are needed because the leads of the diodes physically contact the working fluid (electrolyte). To ensure the generated electro-osmosis is on the diode surface only, the micro-channel height is limited by the height of the SMD (700 μm).

For long-duration real-time microscopic observation of culturing cells in this pumping system, a customized miniature incubator was designed and fabricated to maintain the culturing environment of 37 °C with 5% CO_2 and high humidity. Acrylic was used as the incubator walls (200 mm $\times$ 180 mm $\times$ 40 mm) with inlets for CO_2 and air. A gas flow meter (GD Glass Tube Flowmeters, Key instruments, PA) and a CO_2 sensor (K-33, CO2 Meter, FL) were used to maintain proper CO_2 concentration. The temperature was regulated using a thermal control stage (TCS-100, AmScope, CA) and calibrated using an infrared thermometer (IRT0424, Kintrex, VA). A square (80 mm $\times$ 25 mm) reservoir filled with 2 ml water was installed on a temperature control stage to maintain humidity. This integrated system coupling the proposed culturing platform with live-cell imaging was effectively used for assessing cellular biophysical changes under fluid conditions.[32–35]

B. Characterization of diode pump-driven microfluidics

Characterization of the diode pump flow was performed by tracking fluorescent particles. The seeding particles were 250 nm-radius fluorescent carboxylate-modified particles with excitation wavelength of 505 nm and emission wavelength of 515 nm (Molecular Probes, Lifetechnologies, NY). The particle loading was 0.002 wt. %, evenly stirred in 100 mM sodium chloride or potassium chloride solutions. The pH was adjusted to 7.2 with NaOH and HCl solutions, which is close to cell culture media, e.g., Dulbecco's Modified Eagle Medium (DMEM).[1,30] Two sections of the microchannel—the diode pumping area and the opposite cell culturing area—were monitored by the imaging system to track the movement of the fluorescent particles and to observe cell growth, respectively, (Figure 1(a)). The imaging system included a Nikon Eclipse T1 inverted microscope with a 10$\times$ objective lens, a light source (X-Cite® 120, Lumen Dynamics, Canada), a Nikon ET-GFP filter cube (EX 450/490, DM 495, EM 500/550), an electron-multiplying CCD camera (QuantEM 512SC, Photometrics, AZ) and Nikon NIS-elements software. Due to the fact that the temperature gradient can affect the fluid flow, infrared thermography (Mikrospec) with a resolution of 0.1 °C/pixel was used to monitor temperature distribution for 1 h while the diode pumps were operated at 10 Vpp/cm with 1 kHz in the microchannel. The temperature remained at 25.1 $\pm$ 0.1 °C across and along the entire microchannel during the tests.

Sine wave AC signals were generated using a function generator (Model 33120 A, Agilent Technologies, CO) and a high voltage amplifier (Model 2340, TEGAM, OH) via needle electrodes. DC bias was eliminated and the signal was kept symmetric in order to avoid DC EOS.

Before measuring the flow fields, enough time was given to prevent external fluctuations, which were identified by examining the Brownian motions of the fluorescent nanoparticles. Videos were taken near the diode and on the main stream part of the microchannel to observe the local and global flow patterns, respectively. Images were taken at 14.79 frames per second with an exposure time of 60 ms and the average interval time of about 7 ms. Velocity fields and flow rates were calculated based on a particle tracking velocimetry (PTV) method using ImageJ (National Institute of Health), as the experimental frequency and voltage, i.e., potential, were controlled from 0.1 Hz to 1 MHz and 0.5 Vpp/cm to 10 Vpp/cm, respectively. Transient time was measured when the flows reached a steady state, in which flows were fully developed flow, i.e., a constant flow condition was observed in the opposite side of the diode section, called the "cell culturing optical observing section."

C. *In vitro* culturing A459 cells in the diode pumping platform

In order to identify the biocompatibility of the diode pump platform and the effects of EOF on cell growth, three groups of A549 lung cancer cells were inoculated into a culture dish and two PDMS micro-channels undergoing either syringe pump-driven (∼28 nl/s) or diode pump-driven fluid flows. These three groups are, respectively, the negative (static condition) and positive control groups and the experimental group. A549 cells were cultured in DMEM (Fisher Scientific, MA) complemented with 10% FCS (Thermal Scientific, MA) and 1% penicillin streptomycin (Lifetechnologies, NY) until sufficient cells were available. The cells were cultured in our customized microscopic incubator and observed for 34 h using phase contrast microscopy (PCM). Briefly, the microchannel was autoclaved at 120 °C for 30 min before A549 cells were inoculated at a concentration of 10^5 cells/ml. The cells were cultured in the microchannel for approximately 6 h without flows, followed by replacing the medium prior to applying flows. An AC potential of 12.5 Vpp/cm (10 Vpp in 8 mm between two electrodes) with 10 kHz was applied to the two electrodes to activate the diodes.

III. RESULTS AND DISCUSSION

A. Fluidic characterization of diode pump-driven flows using high-concentration saline solutions

It was found that the flow rate, transient time and flow direction could be controlled by applying specific AC signals with various amplitudes (Figure 2(a)) and frequencies (Figure 2(b)) on the electrodes. Average flow rates monotonically increased with respect to applied electric field when higher than 0.5 Vpp/cm through 10 Vpp/cm, while the flow rates were approximately 2 nl/s when the electric field applied was lower than 1 Vpp/cm (Figure 2(a)). The
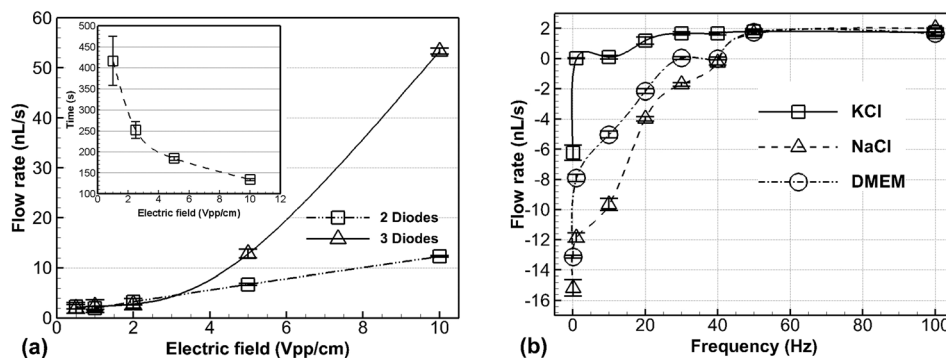

FIG. 2. Experimental characterization of fluidics. (a) In a 100 mM NaCl solution, flow rates and transient time (subset graph) increased and decreased, respectively, as electric field intensity increased up to 20 Vpp/cm (data above 10 Vpp/cm not shown because electrolysis occurred and bubbles blocked the channel). Operating frequency was 1 kHz. (b) Flow rates and directions changed at different operating frequencies for three solutions: sodium chlorine, potassium chlorine, and DMEM. The electric field of 10 Vpp/cm was applied for this experiment.

transient time needed to fully develop the steady flows decreased as the applied voltages increased (subset of Figure 2(a)) from 417 s at 0.5 Vpp/cm to 132 s at 10 Vpp/cm for the two-diode configuration. This range of transient time is negligible compared to the application duration of fluid flows for culturing cells (more than 4 h), so our diode pumps can apply steady flows to stimulate cells. The trend of the change of transient time for three diodes was the same and the duration was shorter (data not shown).

In the three-diode approach, the additional diode was found to be able to highly increase the flow rates especially at high voltages. For example, three diodes generated approximately 53.35 nl/s at 10 Vpp/cm, whereas 12.28 nl/s for two diodes at the same field intensity. This suggests that increased SMD surface area leads to larger EOF. These results also indicate that the AC diode pumping system can accurately control fluid flows at ultra-low flow rates. In our analysis, two possible factors of wall roughness and wall charge capacitance were neglected since they are relatively small in EOF. According to the Helmholtz-Smoluchowski equation,[36] a strong electric field can generally increase fluid flow rate. However, the high saline concentrations in the cell culture medium are out of range for a traditional AC EOS microfluidic system.[26,27] The electric double layer gets thinner, as the salt concentration of solution is higher.[36] In the thinner double layer, the relatively low voltage can generate ultra-low flow rate.

Particle tracking velocimetry (Figure 3(a)) (multimedia view) reveals circulation of nanoparticles near the diodes, indicative of EOS phenomena. In contrast, flow downstream from the diode pumping section was steady and one dimensional (Figure 3(b), multimedia view). A quick flow response was observed that it immediately stopped at the last moment of the movie (Figure 3(b)) by turning off the input power. It demonstrates the accurate flow control.

DMEM culture medium used to culture A549 cells contains many kinds of ions that have different chemical properties and electronegativity (or electropositivity).[37] Due to this characteristic, the operating frequency, i.e., the frequency of AC field applied on the electrodes, and the corresponding flow rates for the DMEM medium should be influenced by ions' charging and releasing mechanisms.[38] Our results were consistent with this theory and suggested the operating frequency should be high enough to control the flow in a designed direction. Specifically, Figure 2(b) illustrates that flow rates vary with different frequencies for three different solutions, 100 mM potassium chloride (KCl), 100 mM sodium chloride (NaCl), or DMEM culture medium. The flow turnover frequency, that is, the frequency at which the direction of flow
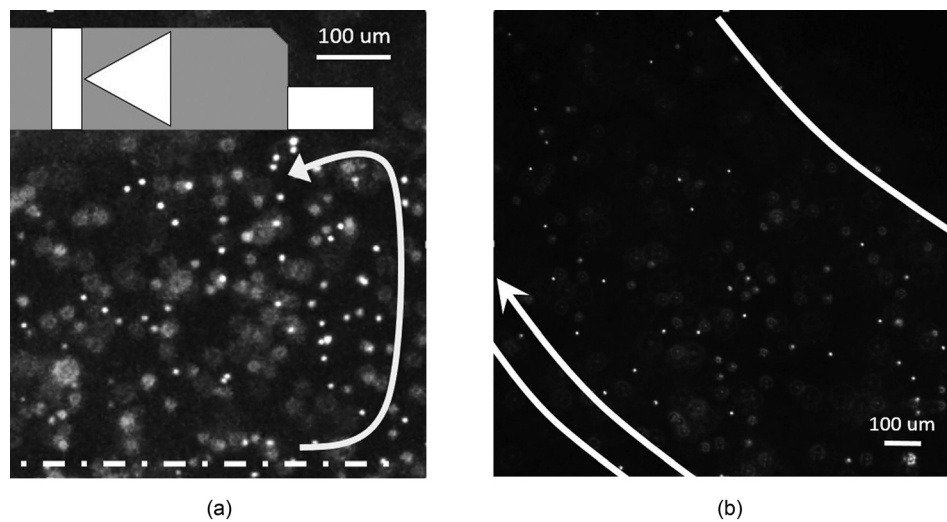

(a)   (b)

FIG. 3. First snapshots from the videos showing movement of fluorescent nanoparticles driven by diode pumps in 100 mM NaCl saline. An AC with Vpp = 25 V was applied at a frequency of 1 kHz. Local vortexes occurred near the diode, where the EOF clearly moved toward left near the surface of the diode (a). The downstream flow exhibited a lamina flow pattern (b). The arrows in (a) and (b) indicate the flow direction. (Multimedia view) [URL: http://dx.doi.org/10.1063/1.4892894.1] [URL: http://dx.doi.org/10.1063/1.4892894.2].

changes—was observed to be at 1 Hz and 42 Hz for KCl and NaCl, respectively, and 30 Hz for the DMEM medium. It is reasonable that the operating frequency trend of DMEM is similar to that of 100 mM NaCl since NaCl is the dominant component in the DMEM medium.[30]

Preliminary experiments performed using this system confirm that the duty cycle can control the flow direction and create pulsatile flows.[39] However, duty-cycles should be maintained at 50%, keeping the signals of the entire channel in AC mode to prevent unwanted electrolysis in the culture medium. Additionally a frequency of more than 1 kHz can be employed to avoid biological effects that occur at low frequencies.[40,41]

The diode pumps can be applied to saline solutions more than 100 mM, while traditional planar electrodes to generate AC EOS flows are limited to liquid solutions with less than 10 mM of salt. Bazant *et al.*[42] proposed a relationship for the electrolyte dependence of the AC-EOF. Using Poisson-Boltzmann theory, a dilute solution of point-like ions in thermal equilibrium in the mean potential suggested a maximum concentration (10 mM), which limits a diffuse-lay voltage. In the dilute solution, the thermal voltage is about 25 mV, which was significantly smaller than typical voltages applied to the double layer in AC-EOS.[43] In the diode-pumping system, application of this small voltage was sufficient to generate EOF and ultra-low flow rates.

The shape of the AC signal is significant and the sine wave is favorable for a diode pump. Owing to the inherent characteristics of the diode to rectify AC signals into pulsed DC signals, the applied voltage was reduced to half. In general, voltage overshoot can create an asymmetric and unpredictable DC current that may generate electro-chemical reactions.[44] Square wave voltage signals exhibited these overshoot voltages (results not shown), while sine waves did not. Although the flow rates generated by a sine wave were slightly lower than those by a square wave at the same voltage input, because the root mean square voltage (V_{rms}) of the sine wave is $\frac{1}{\sqrt{2}}$ times lower than the square wave, the sine wave generates a more consistent flow than does the square wave.

Surface charge plays a significant role in determining the direction of EOS flows. The charge interactions within the Debye length were accounted for from the diode surface (acrylonitrile-butadiene-styrene, ABS) and the glass substrate, whereas the plasma-treated PDMS channel walls are free of charge.[45] Even though negative surface charges on the glass substrate and the diode ABS surfaces are known to be weakly conducting,[29,46,47] positive charges in the electrolyte (KCl, NaCl, or culture medium) will be attracted to the negatively charged surface, resulting in negative charges moving toward the positive tip of the diode, i.e., the direction of EOS flow.

Ferry *et al.* proposed the frequency dependence of the capacity of a diffuse double layer.[48] At low frequencies, the ions are fully polarized and generate maximum driving forces. At a low frequency condition giving more charging time to ions, electrophoresis is more dominant, which is not favorable due to chemical reactions by polarized ions than EOS created by the diode pump. With more complex media, the ionic polarization became more complicit and even more difficult to control. Thus it is better to avoid low frequencies (100 Hz or lower when 10 Vpp/cm was applied) for the cell culture platform application.

B. CFD simulation of diode pump-driven fluidics

In addition to experimental characterization, one DCEO simulation was performed using the CFD code CFD ACE + CFD simulation of DC-EOS illustrates the fluidic profile (when pH = 7.3) near the diode pumping region (Figure 4(a)). Electro-osmotic flow refers to the bulk motion of an aqueous solution past a stationary solid surface because of an externally applied electric field. It requires the presence of a charged double-layer at a solid-liquid interface. For the simulation, the fluid is assumed Newtonian, incompressible, and dilute. Another assumption is that the double layer is very thin and subsequently layer relaxation and distortion can be ignored, indicating that ion convection effects are neglected. The Navier-Stokes equations including the body force and the continuity equation were used for simulation as follows:
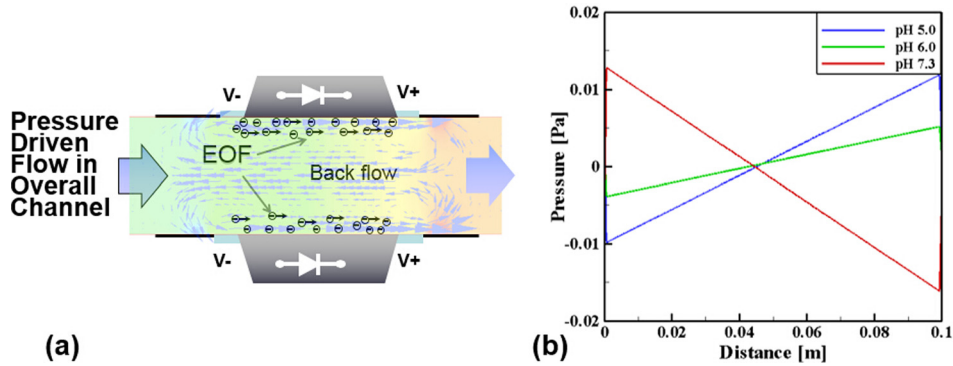
FIG. 4. Fluidic simulation for two diodes by CFD ACE+. (a) Fluidic characteristics in the diode pumping section (pH = 7.3) and (b) pressure distribution along the channel (total length of the loop of channel is 0.1 m, starting from pumping section) at different pH values. Note that the length of overall channel for CFD was 0.1 m, not 0.16 m as used for experimental setting.

$$\rho(\vec{V} \cdot \nabla)\vec{V} = -\nabla P + \mu \nabla^2 \vec{V} + \varepsilon \kappa^2 \varsigma \nabla \phi,$$

$$\nabla \cdot \vec{V} = 0,$$

where ς means the zeta potential ($+60$ mV, $+25$ mV, and -80 mV for pH = 5.0, 6.0, and 7.3, respectively) and ϕ indicates the externally imposed electric potential (10 V). Also, κ is the inverse of Debye thickness which was kept constant at 1×10^7 m and ε is the permittivity. The related electrical conductivity is 5.5E-6 (S/m) and the relative permittivity is 78.5. As shown in Fig. 4(a), the two-dimensional channel was adopted for the current simulation and the computational grid system was constructed by using ICEM-CFD commercial code. For a grid having 45,135 elements determined from the preliminary tests, the solution was found to be grid-independent. The top and bottom surfaces were treated as the no-slip condition and especially on the diode surfaces, the body force related to the electro-osmotic flow was included by using the values of the electric potential, the zeta potential, and relative permittivity. In addition, the pressure boundary conditions are applied at the both ends of the diodes. The governing equations were solved with the SIMPLE algorithm for pressure-velocity coupling. Using the computer with two nodes (2.26 GHz and 4GB memory), the convergence time is about 10 min and the tolerance was taken 0.0001 for all residuals of mass and linear momentum.

Two vortices were observed and a pressure drop is generated. Simulations also demonstrated a variation in pressure gradient along the entire channel for different pH values (Figure 4(b)), which can result in change of the flow rates pumped by the diodes.[29] The direction of circulating flows along the close-loop microchannel was found to be the same as that of the local EOS flows near the diode surfaces (from the anode to the cathode, that is the same direction seen in the experiment) when pH values were lower than 7. In contrast, in a solution with the higher pH, the flow direction was reversed due to the recharging of the diode's surface.

There are counter electro-osmotic pressure gradients across the diode's electrodes because the localized EOF occurs only on the surface of the embedded diodes. Pressure difference depends on pH values, and a linear decrease in static pressure was observed along the flow direction in the rest of the channel (Figure 4(b)). In fact, pressure difference increased with the increase in electrical potentials and viscous forces. Initially stationary fluids begin to move along the diode surfaces due to EOS ionic fluxes. Because of various mean shear rates generated by the diodes away from the diode surfaces, opposing circulation zones are formed. Existence of mean shear rate indicates momentum deficit. For instance as seen in Figure 4(a), the fluid flows (for the pH = 7.3 case) were generated in the positive direction near the surfaces and then mixed with each other in the middle of the channel between two diodes.

In Figure 4(a), a circulating flow region, similar to a closed body shape (like a Rankine oval for potential flows), was observed. Under ideal conditions such as potential flows, two

identical vortices with opposite directions are not able to create the main stream along the channel because, ideally, angular momentum and circulation are conserved. For viscous flows, however, the momentum deficit due to the viscous effect substantially changed the static pressure fields, which eventually generated main stream flows in the closed loop channel. Therefore, it can be concluded that (1) the present flow is initially characterized by shear-driven flows and shows transient phenomena, (2) as the flows reach steady state, the vortex flows are generated in the diode pumping region and the momentum deficit due to viscosity makes the change of static pressure in the downstream direction, and (3) the pressure-driven flows are generated under the steady-state condition along the closed-loop channel.

C. Stability of EOS by diode pumps

The durability of the diode pumping system was also tested in the DMEM medium. The diode pump operated reliably for more than 40 h. The voltage potential between the ends of the diodes was found to decrease from 4.5 Vpp to 1.2 Vpp in DMEM medium when a constant voltage input of 5 Vpp/cm was applied. The diode potential was partially but almost fully recovered after replacing the medium as shown in Figure 5(a). When the medium was changed every hour a relatively constant potential could be maintained (Figure 5(b)). This latter observation demonstrates the feasibility of the diode pumping system as a long duration *in vitro* cell culture platform. Cell culture medium consists of complex chemical components. The long-term application using the external field with even smaller voltage would induce the deposition of chemicals on the electrodes, which increased the resistance. Therefore, the increased resistance caused the voltage drop of working voltage potential. An unknown coating was observed on the diodes by using an optical microscopy after the experiment (data not shown). Therefore, replacing with the fresh medium can help the system recover the potential (seen in Fig. 5(a)) and cyclic medium replacement keeps the diode potential almost constant (seen in Fig. 5(b)).

D. Effects of diode pump-driven flows on cells

By culturing A549 cells in the diode pumping platform, it was observed that the diode pump could positively affect cell growth in a similar manner to a syringe pump platform. The cells grew morphologically better in dynamic fluidic environments of diode pumping and syringe pumping systems and were morphologically similar to those in the syringe pumping setup (Figures 6(b) and 6(c)). Cells in both cases adhered more tightly to each other than those in the conventional culture dish (Figure 6(a)). Note that if an AC electric field of 12.5 Vpp/cm with maximum peak voltage of 10 V is applied to activate a pair of diodes in a channel with a total length of 16 cm, the current in the medium in the channel was calculated approximately as 0.1 μA by using Ohm's law. The resulting resistance was calculated as 95.8 MΩ, by knowing
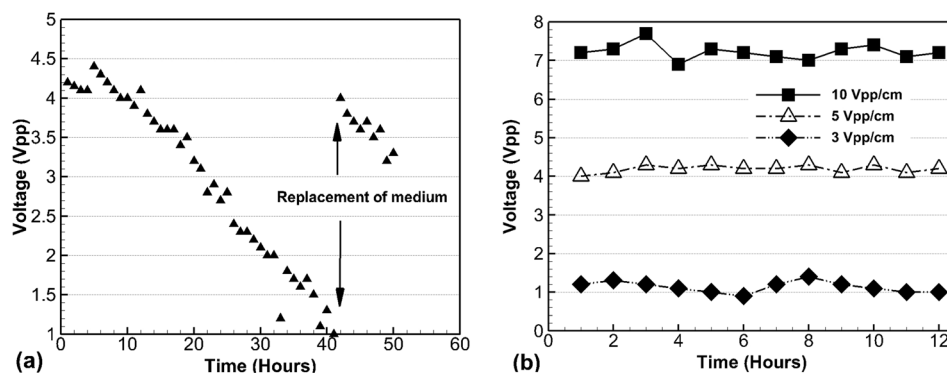

FIG. 5. Time-dependent voltage changes in DMEM medium during diode pumping. Voltages measured between the ends of the diode decreased over time and return back after changing medium at 40 h, where 5 Vpp/cm was applied (a). Real time monitoring voltages were kept constant for fixed applied electric field as long as the DMEM medium was replaced every hour (b).
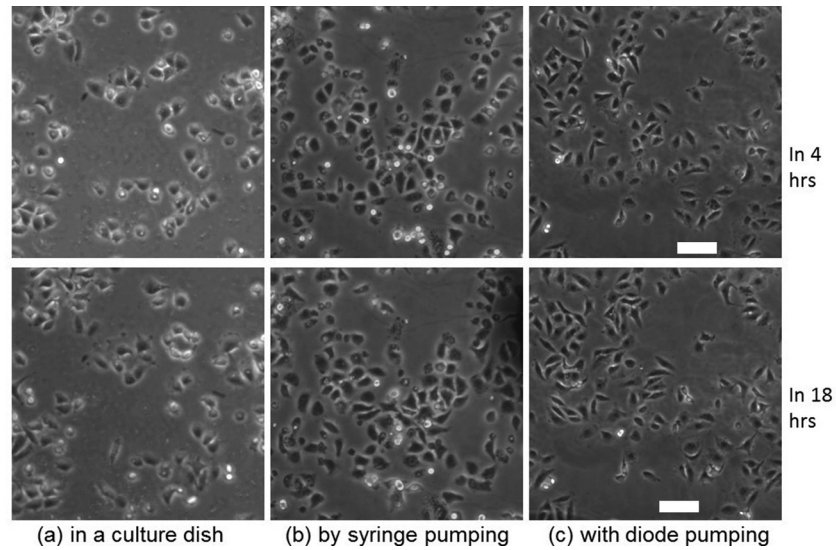
FIG. 6. Time lapse PCM images of A549 cells grown in a culture dish (a) and in PDMS micro-channels with syringe pumping (b) or diode pumping (c). Images were selected from 4 h (top row) or 18 h (bottom row). Scale bar = 75 μm.

the medium conductivity, the cross sectional area of the microchannel and the entire length of microchannel. This current is considerably below the amperage that causes cellular disruption.[49,50] This result also demonstrates that the localized EOS near the diodes caused no adverse effects on the cell.

Traditional pumping systems, albeit popular, are not particularly accurate and require bulky equipment compared to the diode pumping system demonstrated here. The diode pump can precisely generate ultra-low volume flow rates that may be required to culture specific adherent cells.[51] Continuous and pulsatile flows, which more accurately represent the natural and dynamic flow of the cardiovascular system, can also be regulated using this system, by controlling the time delay. This diode pumping system can also be significant for studies focusing on the effects of ultra-low flows in the field of cartilage tissue engineering.[51] Compared to the flow rate range our pump can reach, commercial peristaltic pumps employed in the literature still generate too high flow rates ($\sim$1 μl/min).[51] While the cost of a micro-fabricated device will be higher than a Petri dish used in traditional cell-culturing systems, the overall cost of employing our system can be lower due to system miniaturization, low power consumption, and reduction in medium consumption. Moreover, this pumping system can be integrated with an automated microscopy incubator due to its small size.

Not only does this novel microfluidic culture platform better mimic *in vivo* flow conditions, media recirculation economizes culture media and treatment compounds[52] while significantly reducing cost. Additionally, when a multimodality imaging system[53,54] is coupled with the culture platform, data can be collected on morphological cell changes under dynamic conditions/ treatments. The microfluidic cell culture system holds great promise for the creation of advanced cell culture models, as it will facilitate control of the spatial distribution and temporal response of cells and biomolecules.

IV. SUMMARY AND FUTURE PERSPECTIVES

A cell culture platform that utilizes a diode pumping system to induce dynamic fluid flows was developed. We, for the first time, employed diodes to generate flows in saline solutions and culturing medium whose concentrations were greater than 100 mM. The intensity, frequency, and wave shape of electric input have been tested and optimized. The ultra-low flow rates were as small as 2 $\sim$ 12 nl/s that cannot be generated by hydrodynamic syringe pumps. We also demonstrated the biocompatibility of this system compared to a commercial syringe

pump. Due to the small size, the diode pumping system could be integrated with a microscopy incubator, which suggests its potential for lab-on-a-chip applications and real time monitoring advantages. Though by changing the medium every hour, this system can be used for a long term, further study is needed to address the effects of chemical reaction in culture medium in order to reduce human labor.

ACKNOWLEDGMENTS

[1] R. I. Freshney, *Culture of Animal Cells: A Manual of Basic Technique and Specialized Applications* (Wiley, 2011).

[2] M. C. Phelan, "Basic techniques in mammalian cell tissue culture," *Current Protocols in Cell Biology* (Wiley, 2007), Chap. 1.

[3] J. J. Gunderson and J. C. Giddings, "Chemical composition and molecular-size factors in polymer analysis by thermal field-flow fractionation and size exclusion chromatography," Macromolecules **19**(10), 2618–2621 (1986).

[4] Z.-D. Shi and J. M. Tarbell, "Fluid flow mechanotransduction in vascular smooth muscle cells and fibroblasts," Ann. Biomed. Eng. **39**(6), 1608–1619 (2011).

[5] J. N. Topper and M. A. Gimbrone, "Blood flow and vascular gene expression: fluid shear stress as a modulator of endothelial phenotype," Mol. Med. Today **5**(1), 40–46 (1999).

[6] J. S. Garanich *et al.*, "Effects of fluid shear stress on adventitial fibroblast migration: Implications for flow-mediated mechanisms of arterialization and intimal hyperplasia," Am. J. Physiol.: Heart Circ. Physiol. **292**(6), H3128–H3135 (2007).

[7] C. P. Ng and M. A. Swartz, "Fibroblast alignment under interstitial fluid flow using a novel 3-D tissue culture model," Am. J. Physiol.: Heart Circ. Physiol. **284**(5), H1771–H1777 (2003).

[8] S. P. Fritton and S. Weinbaum, "Fluid and solute transport in bone: Flow-induced mechanotransduction," Annu. Rev. Fluid Mech. **41**, 347–374 (2009).

[9] P. M. Govey *et al.*, "Integrative transcriptomic and proteomic analysis of osteocytic cells exposed to fluid flow reveals novel mechano-sensitive signaling pathways," J. Biomech. **47**(8), 1838–1845 (2014).

[10] T. Chen *et al.*, "Insights into interstitial flow, shear stress, and mass transport effects on ECM heterogeneity in bioreactor-cultivated engineered cartilage hydrogels," Biomech. Model. Mechanobiol. **11**(5), 689–702 (2012).

[11] T. Mawatari *et al.*, "Effects of tensile strain and fluid flow on osteoarthritic human chondrocyte metabolism *in vitro*," J. Orthop. Res. **28**(7), 907–913 (2010).

[12] L. Haiwang *et al.*, "Microfluidic on-chip fluorescence-activated interface control system," Biomicrofluidics **4**(4), 044109 (2010).

[13] J. Shendure and H. Ji, "Next-generation DNA sequencing," Nat. Biotechnol. **26**(10), 1135–1145 (2008).

[14] M. M. Wang *et al.*, "Microfluidic sorting of mammalian cells by optical force switching," Nat. Biotechnol. **23**(1), 83–87 (2005).

[15] M. L. Cantwell, F. Amirouche, and J. Citerin, "Low-cost high performance disposable micropump for fluidic delivery applications," Sens. Actuators, A **168**(1), 187–194 (2011).

[16] O. C. Jeong and S. Konishi, "Fabrication and drive test of pneumatic PDMS micro pump," Sens. Actuators, A **135**(2), 849–856 (2007).

[17] C. Koch, V. Remcho, and J. Ingle, "PDMS and tubing-based peristaltic micropumps with direct actuation," Sens. Actuators, B **135**(2), 664–670 (2009).

[18] J. Steigert *et al.*, "Integrated sample preparation, reaction, and detection on a high-frequency centrifugal microfluidic platform," J. Assoc. Lab. Autom. **10**(5), 331–341 (2005).

[19] M. M. Teymoori and E. A. Abbaspour-Sani, "A novel electrostatic micromachined pump for drug delivery systems," in *Proceedings of ICSE 2002, IEEE International Conference on Semiconductor Electronics* (Semiconductor Electronics, 2002).

[20] J. C. Rife, *et al.*, "Miniature valveless ultrasonic pumps and mixers," Sens. Actuators, A **86**(1–2), 135–140 (2000).

[21] M. E. Moghadam and M. B. Shafii, "Rotary magnetohydrodynamic micropump based on slug trapping valve," J. Microelectromech. Syst. **20**(1), 260–269 (2011).

[22] A. Khademhosseini *et al.*, "Microscale technologies for tissue engineering and biology," Proc. Natl. Acad. Sci. U.S.A. **103**(8), 2480–2487 (2006).

[23] X. Wang *et al.*, "Electroosmotic pumps and their applications in microfluidic systems," Microfluid. Nanofluid. **6**(2), 145–162 (2009).

[24] C.-C. Huang, M. Z. Bazant, and T. Thorsen, "Ultrafast high-pressure AC electro-osmotic pumps for portable biomedical microfluidics," Lab Chip **10**(1), 80–85 (2010).

[25] Y. M. Senousy and C. K. Harnett, "Fast three dimensional ac electro-osmotic pumps with nonphotolithographic electrode patterning," Biomicrofluidics **4**(3), 036501 (2010).

[26] M. Z. Bazant and Y. Ben, "Theoretical prediction of fast 3D ac electro-osmotic pumps," Lab Chip **6**(11), 1455–1461 (2006).

[27] J. P. Urbanski *et al.*, "Fast ac electro-osmotic micropumps with nonplanar electrodes," Appl. Phys. Lett. **89**(14), 143508 (2006).

[28] D. Li, *Encyclopedia of Microfluidics and Nanofluidics* (Springer, 2008).

[29] S. T. Chang *et al.*, "Remotely powered distributed microfluidic pumps and mixers based on miniature diodes," Lab Chip **8**(1), 117–124 (2008).

[30] L. Rutzky and R. Pumper, "Supplement to a survey of commercially available tissue culture media (1970)," In Vitro **9**(6), 468–469 (1974).

[31] A. M. Christensen, D. A. Chang-Yen, and B. K. Gale, "Characterization of interconnects used in PDMS microfluidic systems," J. Micromech. Microeng. **15**(5), 928–934 (2005).

[32] E. W. Young and D. J. Beebe, "Fundamentals of microfluidic cell culture in controlled microenvironments," Chem. Soc. Rev. **39**(3), 1036–1048 (2010).

[33] M. L. Kovarik *et al.*, "Micro total analysis systems for cell biology and biochemical assays," Anal. Chem. **84**(2), 516–540 (2012).

[34] E. W. Young and C. A. Simmons, "Macro-and microscale fluid flow systems for endothelial cell biology," Lab Chip **10**(2), 143–160 (2010).

[35] S. Kim, H. J. Kim, and N. L. Jeon, "Biological applications of microfluidic gradient devices," Integr. Biol. **2**(11–12), 584–603 (2010).

[36] B. Kirby, *Micro- and Nanoscale Fluid Mechanics* (Cambridge University Press, 2010).

[37] X. Yan *et al.*, "Lung cancer A549 cells migrate directionally in dc electric fields with polarized and activated EGFRs," Bioelectromagnetics **30**(1), 29–35 (2009).

[38] J.-L. Hong, K.-C. Lan, and L.-S. Jang, "Electrical characteristics analysis of various cancer cells using a microfluidic device based on single-cell impedance measurement," Sens. Actuators, B **173**(0), 927–934 (2012).

[39] S. T. Chang *et al.*, "Remotely powered self-propelling particles and micropumps based on miniature diodes," Nat. Mater. **6**(3), 235–240 (2007).

[40] C. D. McCaig, B. Song, and A. M. Rajnicek, "Electrical dimensions in cell science," J. Cell Sci. **122**(23), 4267–4276 (2009).

[41] E. D. Kirson *et al.*, "Alternating electric fields arrest cell proliferation in animal tumor models and human brain tumors," Proc. Natl. Acad. Sci. U. S. A. **104**(24), 10152–10157 (2007).

[42] M. Z. Bazant, *et al.*, "Electrolyte dependence of AC electro-osmosis," in *Proceedings of 11th International Conference on Miniaturized Systems for Chemistry and Life Sciences, MicroTAS* (Chemical and Biological Microsystems Society, 2007).

[43] M. S. Kilic, M. Z. Bazant, and A. Ajdari, "Steric effects in the dynamics of electrolytes at large applied voltages. I. Double-layer charging," Phys. Rev. E **75**(2), 021502 (2007).

[44] H. Lee, J. H. Jeong, and T. G. Park, "PEG grafted polylysine with fusogenic peptide for gene delivery: High transfection efficiency with low cytotoxicity," J. Controlled Release **79**(1–3), 283–291 (2002).

[45] L. S. McCarty and G. M. Whitesides, "Electrostatic charging due to separation of ions at interfaces: Contact electrification of ionic electrets," Angew. Chem., Int. Ed. **47**(12), 2188–2207 (2008).

[46] L. E. Locascio, C. E. Perso, and C. S. Lee, "Measurement of electroosmotic flow in plastic imprinted microfluid devices and the effect of protein adsorption on flow rate," J. Chromatogr. A **857**(1–2), 275–284 (1999).

[47] G. Dodbiba *et al.*, "The use of air tabling and triboelectric separation for separating a mixture of three plastics," Miner. Eng. **18**(15), 1350–1360 (2005).

[48] J. D. Ferry, "Frequency dependence of the capacity of a diffuse double layer," J. Chem. Phys. **16**(7), 737–739 (1948).

[49] P. M. Ghosh, C. R. Keese, and I. Giaever, "Morphological response of mammalian cells to pulsed ac fields," Bioelectrochem. Bioenerg. **33**(2), 121–133 (1994).

[50] C. R. Keese *et al.*, "Electrical wound-healing assay for cells *in vitro*," Proc. Natl. Acad. Sci. U.S.A. **101**(6), 1554–1559 (2004).

[51] Raimondi, M. T., *et al.*, "Engineered cartilage constructs subject to very low regimens of interstitial perfusion," Biorheology **45**(3–4), 471–478 (2008).

[52] Z.-R. Xu *et al.*, "An osmotic micro-pump integrated on a microfluidic chip for perfusion cell culture," Talanta **80**(3), 1088–1093 (2010).

[53] C. K. Choi *et al.*, "Cell adhesion property affected by cyclooxygenase and lipoxygenase: Opto-electric approach," Biochem. and Biophys. Res. Commun. **391**(3), 1385–1389 (2010).

[54] C. K. Choi *et al.*, "Multicontrast microscopy technique to dynamically fingerprint live-cell focal contacts during exposure and replacement of a cytotoxic medium," J. Biomed. Opt. **13**(5), 054069 (2008).